Conductivity coherence factors in the conventional superconductors Nb and Pb

O. Klein*

Department of Physics, University of California at Los Angeles, Los Angeles, California 90024

E.J. Nicol†

Department of Physics, University of California at Santa Barbara, Santa Barbara, California 93106

K. Holczer and G. Grüner

Department of Physics, University of California at Los Angeles, Los Angeles, California 90024

(Received 29 March 1994)

We have performed microwave measurements at 60 GHz of the surface impedance ($Z_s = R_s - iX_s$) on superconducting Nb and Pb. The temperature dependence of the complex conductivity ($\hat{\sigma} = \sigma_1 + i\sigma_2$) is inferred from the data down to $T/T_c \sim 0.25$ for both materials. The imaginary part, $\sigma_2(T)$, gives the temperature dependence of the superconducting gap and the real part, $\sigma_1(T)$, exhibits the predicted conductivity coherence peak below T_c. The findings are compared with the expressions calculated by Mattis and Bardeen to describe the electrodynamics of weak-coupling BCS superconductors. Furthermore, we calculate the complex conductivity within the framework of the standard Eliashberg electron-phonon theory of superconductivity. The experimental results obtained on Nb are in good agreement with the BCS weak-coupling theory while the data on Pb are analyzed in the anomalous (Pippard) limit and show deviations from BCS laws, accounted for only by the Eliashberg strong-coupling description of the electrodynamics of the superconducting state.

I. INTRODUCTION

The observation of coherence factors by ultrasonic attenuation and by nuclear spin relaxation has provided important confirmation of the BCS theory of superconductivity.[1,2] Those two experiments illustrate in a dramatic way the pairing mechanism in superconductors. The coherence factors are fundamental because they are derived purely from symmetry arguments. The fact that the electrodynamic response reflects also the coherence factors was confirmed in 1967 by Tinkham and co-workers[3] for pair breaking processes where the photon energy, $\hbar\omega$, is larger than twice the single particle gap, 2Δ. The low temperature study ($T \ll T_c$) of the infrared (10–200 cm^{-1}) conductivity spectrum of Pb by Palmer and Tinkham,[4] and by other groups,[5] led to the observation of the slow and monotonic increase of the conductivity (with increasing frequency) at the gap edge and provided convincing evidence that optical absorption processes in superconductors are governed by case 2 coherence factors.[4] Their findings were in excellent agreement with the expression developed by Mattis and Bardeen.[6]

In addition, it is known that the mechanism for superconductivity in conventional superconductors is the electron-phonon interaction.[2] This interaction is manifested in the electromagnetic spectrum by structure in the absorption due to phonon scattering with a particle-hole pair, known as Holstein structure.[7] In superconductors such as Pb, this structure occurs in the infrared spectral range. In the superconducting state, with the opening of the energy gap, the structure is shifted by

2Δ. The magnitude of the Holstein structure depends on the strength of the electron-phonon coupling and the cleanness of the sample. Nam[8,9] first set forth a theory of the conductivity demonstrating the Holstein effect in the calculated conductivity of Pb. He used a generalization of BCS theory known as Eliashberg theory,[10] which incorporates the complete details of the retarded electron-phonon interaction. This theory is known to describe the physical properties of conventional superconductors to within a few percent.[11] Experimentally, Holstein structure has been found in the electromagnetic absorption of Pb by Palmer and Tinkham[4] and Joyce and Richards[12] with very good agreement between experiment and theory.[9,13–15] This has been taken as important confirmation of the electron-phonon interaction giving rise to the superconductivity in conventional superconductors.

Several early experiments focused on the frequency range $\omega \ll \Delta/\hbar$. In 1958, Khaikin[16] studied the electrodynamic properties of Cd at 9 GHz or 0.3 cm^{-1} ($\hbar\omega/2\Delta \sim 0.3$). A few years later, in 1964, Waldram[17] measured the surface impedance of Sn at 3 GHz ($\hbar\omega/2\Delta \sim 0.01$). Both experiments successfully compared their results with the microscopic BCS theory. Subsequent studies by Lehoczky and co-workers were based on measurements of the microwave (24–70 GHz) transmission and reflection coefficients for thin superconducting films of Pb,[18,19] and the inferred $\sigma_1(T)$ was interpreted in terms of fluctuation effects. More recently, microwave studies at 5 GHz were published by Halbritter[20] on the surface resistance of Pb and Nb. He evaluated carefully R_s at low temperatures ($T \ll T_c$)

and studied impurity effects. Again, the data were in good agreement with the existing theory. The coherence effects, however, were never measured at microwave frequencies. The reason for this (as will be discussed later) is clear: In order to extract σ_1, both components of the surface impedance have to be measured to high accuracy.

In this paper we report our surface impedance measurements on the conventional superconductors Nb and Pb. By careful evaluation of both components of the complex impedance, we obtain the two components of the complex conductivity $\hat{\sigma} = \sigma_1 + i\sigma_2$ at a frequency $f = 60$ GHz ($\hbar\omega/2\Delta \sim 0.1$), well below the gap frequency for both materials. In the two cases, we find a peak in $\sigma_1(T)$ which is analogous to the Hebel-Slichter peak[21] found in the nuclear spin lattice relaxation rate, T_1. The organization of this paper is as follows: In Sec. II we will present the current theoretical understanding of the electrodynamics of superconductors. Section III gives a description of the experimental setup. In Sec. IV, we present the results of our measurements and in Sec. V we compare them with theory. Finally in Sec. VI we give our conclusions.

II. ELECTRODYNAMICS OF SUPERCONDUCTORS: A SHORT SUMMARY

At microwave frequencies, the response of a highly conducting specimen is usually measured by the complex surface impedance, $Z_s = R_s - iX_s$, where R_s is the surface resistance and X_s is the surface reactance. The surface impedance is defined[22] as the ratio of the electric and magnetic fields at the surface of the metal $Z_s \equiv E_{\parallel}/H_{\parallel}$, where the $\parallel$ sign indicates the field component in the plane of the surface. It is a unitless quantity, independent of the surface geometry and normalized by the impedance of the vacuum, $Z_0 = 4\pi/c = 377$ Ω, where c is the speed of light. The "surface" impedance measures in fact the bulk properties of the sample as the field penetrates in the material on a length scale, $1/\mathrm{Im}(\hat{k})$, where $\hat{k}$ is the wave vector inside the material. This length (~ 0.5 μm) is either the skin depth in the normal state or the penetration depth in the superconducting phase.

For a superconductor, the relation between the surface impedance and the conductivity depends on the ordering of three length scales: the mean free path, ℓ, the coherence length, ξ, and the penetration depth, λ. These parameters are in general interdependent quantities and all vary with temperature and impurity concentration. The labeling of the different limits is a point of confusion in the literature, as the words are interchanged to describe similar limiting expressions. For clarity, we first define our vocabulary. It is customary to introduce the zero temperature values of λ and ξ in the London (clean) limit:

$$\lambda_L = \frac{c}{\omega_P} \quad \text{and} \quad \xi_0 = \frac{\hbar v_F}{\pi\Delta(0)}, \tag{1}$$

where v_F is the Fermi velocity and $\omega_P = 4\pi n_e e^2/m$ is the plasma frequency. Depending on which is the smallest length scale, a superconductor can be described as falling into one of the three following cases.[11]

(i) *The local limit,* is where $\ell \ll \xi, \lambda$ (independently of whether it is a type I or type II superconductor). More commonly it is also referred to as the *dirty limit* defined by $\ell/\xi \to 0$.

In the opposite, so called *clean limit,* $\ell/\xi \to \infty$, it is necessary to distinguish the following two cases.

(ii) *The Pippard* or *anomalous* limit, defined by the inequality $\lambda \ll \xi, \ell$ (a clean type I superconductor).

(iii) *The London limit* for which $\xi \ll \lambda, \ell$ (a clean type II superconductor).

The important result is that the reduced quantity Z_s/R_n equals $\sqrt{2}(i\hat{\sigma}/\sigma_n)^{-1/2}$ in both the local and London limits.[8] The subscript n indicates the value just above T_c. In the anomalous limit $Z_s/R_n = 2(-\hat{\sigma}/\sigma_n)^{-1/3}$. Finally, it has also been shown[8] that the reduced conductivity $\hat{\sigma}/\sigma_n$ is identical in both the anomalous and the local limits.

The qualitative frequency and temperature dependence of σ_1/σ_n in the superconducting phase can be inferred from the symmetry of the pairing (time reversal) solely, where the answer is classified by the coherence cases. In calculating the matrix elements of an absorption rate by the quasiparticles, one has to take into account that the ground state is occupied by pairs. In the condensed phase, the different states that belong to the same symmetry class interact coherently and give rise to interference effects that would be completely absent in the normal state (independent summation). For time-reversal symmetry, each class is doubly degenerate (Kramer's theorem) and the interference is either destructive (case 1) or constructive (case 2). Experimentally there are two ways to distinguish between the two cases. One can study the low temperature ($T \ll T_c$) spectrum of the absorption rate near the gap edge ($\omega \geq 2\Delta/\hbar$) or measure the temperature dependence of the absorption rate at low frequency ($\omega \ll 2\Delta/\hbar$). The former experiment was done by Tinkham and co-workers[3] and gave evidence that electromagnetic absorption is governed by case 2 coherence factors. However, the conductivity coherence peak predicted by the BCS theory was not established before.

In 1958, Mattis and Bardeen investigated the electrodynamics of superconductors[6] in the Pippard regime, using the approximation that $\tau \gg \hbar/\Delta > \lambda/v_F$ to simplify the algebra. When $\tau \to \infty$ the conductivity expression simplifies to

$$\frac{\hat{\sigma}}{\sigma_n} = \frac{2}{\omega}\int_\Delta^\infty [f(u) - f(u+\omega)]g(u)du + \frac{1}{\omega}\int_{\Delta-\omega}^\Delta [1 - 2f(u+\omega)]g(u)du, \tag{2}$$

where

$$g(u) = \frac{(u^2 + \Delta^2 + \omega u)}{u_1 u_2}, \quad \text{where} \quad \begin{cases} u_1 = \mathrm{sgn}(u)\sqrt{u^2 - \Delta^2}, & |u| > \Delta, \\ = -i\sqrt{\Delta^2 - u^2}, & |u| < \Delta, \\ u_2 = \sqrt{(u+\omega)^2 - \Delta^2}, \end{cases}$$

$$f(u) = 1/[1 + \exp(u/T)].$$

Here, $\omega \equiv \hbar\omega$, $T \equiv k_B T$, and $\Delta \equiv$ BCS gap.

Figure 1 shows the temperature and frequency dependence of σ_1/σ_n as derived from Eq. (2). It reproduces the behavior predicted for case 2 coherence factors and at low frequencies ($\hbar\omega \ll \Delta$), $\sigma_1(T)$ has a peak below T_c. Notice that the peak has completely disappeared for $\hbar\omega \geq \Delta/5$. For the purpose of clarity, the conductivity below $\hbar\omega/\Delta < 0.01$ is omitted in Fig. 1. It seems then that the total area under the curve $\sigma_1(\omega)$ changes below T_c. The oscillator strength sum rule, however, imposes that the total spectral weight of $\sigma_1(\omega)$ is a constant independent of temperature. The "missing area" appears as a δ function at $\omega = 0$ (not shown), which physically represents the superfluid response to a dc field (the Meissner effect). It is clear that the amplitude of the δ function depends on the value of the gap. The section along the frequency axis was compared to the infrared measurements of Tinkham and co-workers.[4] We will compare our microwave results, conducted at a single frequency, with the sections along the temperature axis. The temperature dependence of the single particle gap corresponds to the cusp in the surface.

The conductivity coherence peak, $\sigma_1(T)$ at $\hbar\omega \ll \Delta$, is characterized both by its width (the full width at $\sigma_1/\sigma_n = 1$) and its amplitude ($\sigma_1/\sigma_{n\,\mathrm{max}}$). It can be shown that a small increase of Δ (e.g., 10%) in Eq. (2) produces a noticeable decrease ($\sim 10\%$) of the peak width. One could model deviations from the BCS weak-coupling theory by assuming $\Delta(0)/k_B T_c$ to be a free parameter and using the Mattis-Bardeen expression to analyze the experimental results. Obviously such an approach neglects many features of the strong-coupling limit. Therefore, in the analysis below, we have used the full Eliashberg theory to account for strong-coupling effects and kept the BCS coupling value [$\Delta(0)/k_B T_c = 1.76$] in the Mattis-Bardeen expression. The height of the peak depends on the smearing of the singularity in the density of states (a complete discussion can be found in Ref. 23, p. 135). The smearing is parametrized by a lower cutoff energy in the excitation density of states: It is the

probing frequency[24] in the Mattis-Bardeen formula and the amplitude $(\sigma_1/\sigma_n)_{\mathrm{max}} \sim \ln(2\Delta/\hbar\omega)$.[24] The peak height yields, in principle, the magnitude of the gap. Note, however, that lifetime effects (as expected in a real metal) would smear out also the logarithmic divergence as $\omega \to 0$, as is the case for the coherence peak in the temperature dependence of the NMR relaxation rate. Finally, we recall that Hebel[25] fit the coherence peak of the NMR relaxation rate by assuming an anisotropy in the gap distribution.

The corresponding expression for the conductivity in the full strong-coupling Eliashberg theory is more complicated than the BCS expression, with the main feature being that there is now a complex and frequency-dependent renormalization function, $Z(\omega) = Z_1(\omega) + iZ_2(\omega)$, and gap function, $\Delta(\omega) = \Delta_1(\omega) + i\Delta_2(\omega)$. Here the energy gap Δ_0 is defined from $\Delta_0 = \Delta_1(\omega = \Delta_0)$ and $Z_1(\omega = 0) \approx 1 + \lambda_{ep}$, where λ_{ep} is the electron-phonon mass renormalization parameter related to the electron-phonon spectral density $\alpha^2 F(\omega)$ by $\lambda_{ep} = 2\int_0^\infty d\omega \alpha^2 F(\omega)/\omega$. The weak-coupling BCS limit would correspond to $Z(\omega) = 1$ and $\Delta(\omega) = \Delta_0$ up to some cutoff energy of about ω_D, the Debye energy, and zero thereafter.

The method of solution for the $Z(\omega)$ and $\Delta(\omega)$ is well documented in the literature and therefore we will not reproduce the lengthy details here. The basic procedure involves a numerical solution of the nonlinear, coupled Eliashberg equations. One can solve the real frequency axis equations as was done originally,[26,27] or do as we have done and solve the imaginary frequency axis equations[28,29] for $\Delta(i\omega_n)$ and $Z(i\omega_n)$ and perform an analytic continuation[30] to obtain $\Delta(\omega)$ and $Z(\omega)$.

The optical conductivity is then calculated from an expression which is similar to the expression used by Nam,[9] and Swihart and Shaw,[14] but allows for arbitrary impurity scattering, a case of current interest in the literature. Recent derivations can be found.[31,32] In this case the optical conductivity is given as

$$\hat{\sigma}(\nu) = \frac{\omega_p^2}{8\pi\nu}\left\{\int_0^\infty d\omega \tanh\frac{\beta\omega}{2}\frac{[1 - N(\omega)N(\omega+\nu) - M(\omega)M(\omega+\nu)]}{-i\epsilon(\omega) - i\epsilon(\omega+\nu) + 1/\tau}\right.$$

$$+ \int_0^\infty d\omega \tanh\frac{\beta(\omega+\nu)}{2}\frac{[1 - N^*(\omega)N^*(\omega+\nu) - M^*(\omega)M^*(\omega+\nu)]}{-i\epsilon^*(\omega) - i\epsilon^*(\omega+\nu) - 1/\tau}$$

$$+ \int_0^\infty d\omega \left[\tanh\frac{\beta(\omega+\nu)}{2} - \tanh\frac{\beta\omega}{2}\right]\frac{[1 + N^*(\omega)N(\omega+\nu) + M^*(\omega)M(\omega+\nu)]}{i\epsilon^*(\omega) - i\epsilon(\omega+\nu) + 1/\tau}$$

$$+ \int_{-\nu}^0 d\omega \tanh\frac{\beta(\omega+\nu)}{2}\left[\frac{[1 - N^*(\omega)N^*(\omega+\nu) - M^*(\omega)M^*(\omega+\nu)]}{-i\epsilon^*(\omega) - i\epsilon^*(\omega+\nu) - 1/\tau}\right.$$

$$\left.\left.+ \frac{[1 + N^*(\omega)N(\omega+\nu) + M^*(\omega)M(\omega+\nu)]}{i\epsilon^*(\omega) - i\epsilon(\omega+\nu) + 1/\tau}\right]\right\}, \tag{3}$$
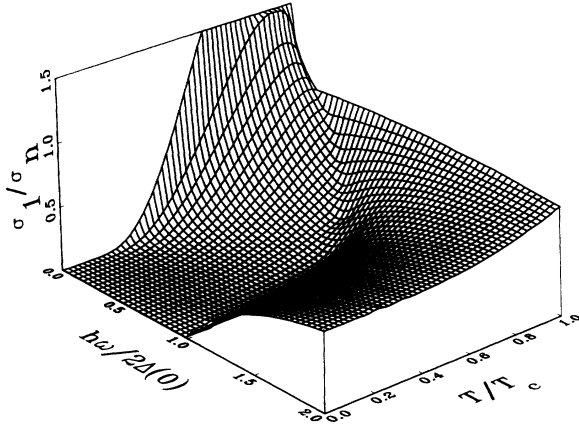
FIG. 1. Temperature and frequency dependence of the conductivity $\sigma_1(T,\omega)$ as evaluated from the Mattis-Bardeen expression, Eq. (2). The coherence peak exists only at low frequencies $\hbar\omega/2\Delta(0) < 0.1$. The cusp in the surface is the energy gap.

where $\beta = 1/T$, $\epsilon(\omega) = \sqrt{\tilde{\omega}^2 - \tilde{\Delta}(\omega)^2}$, $\epsilon(-\omega) = -\epsilon^*(\omega)$, with $\tilde{\omega} \equiv \omega Z(\omega)$, $\tilde{\Delta}(\omega) \equiv Z(\omega)\Delta(\omega)$, $N(\omega) = \tilde{\omega}/\epsilon(\omega)$, and $M(\omega) = \tilde{\Delta}(\omega)/\epsilon(\omega)$. The parameter $1/\tau$ is the elastic impurity scattering rate which we will take to be infinite here as this gives the correct limit for Nb (local limit, as discussed below) and Pb (anomalous limit, which as indicated above is equivalent to the local limit for this quantity). In addition, it has already been shown that unless the impurity scattering is very small, approaching the very clean limit, the calculation will give the dirty limit result for $\hat{\sigma}/\sigma_n$.[33,34]

III. EXPERIMENTAL METHOD: CAVITY PERTURBATION

To measure the surface impedance, we have used a cavity perturbation technique. A recent review of the subject can be found in the article of Portis et al.[35] or Klein et al.,[36] and the references cited therein. The cavity resonance is characterized both by the center frequency, $f_0 = \omega_0/2\pi$, and width Γ (or quality factor $Q = f_0/\Gamma$) of the power absorption spectrum:[37]

$$A(\omega) = \frac{1}{4(\omega - \omega_0)^2 + (2\pi\Gamma)^2}. \qquad (4)$$

The Lorentzian spectrum is expressed in the time domain by a complex resonance frequency $\hat{\omega} = \omega_0 - i\omega_0/2Q$, where all fields have a time dependence of the form $\exp(-i\hat{\omega}t)$.

The resonator used in this study is a cylindrical copper cavity working in the TE_{011} mode; its height is equal to 4.77 mm and its diameter is 7.15 mm. The advantage of this mode is that it has only circumferential currents and thus it minimizes contact problems between the removable end plates and the cavity body. Although the highest Q resonators are achieved with undercoupled cavity in which the reflected signal is detected, the base line

distortions due to standing waves become so large at 60 GHz that we employ a transmission cavity where an isolator is inserted in front of the Shottky diode (detector).

Most techniques using resonant cavities measure the influence of a foreign body on the characteristics of the resonator. For metals, the variation of the complex frequency (measured from the notional perfect conducting state of the sample; i.e., the same body is a loss-free object: $Z_s = 0$ or $|\hat{\sigma}| \to \infty$) is, at first order, proportional to the surface impedance of the specimen $\Delta\hat{\omega}/\hat{\omega} \equiv -i\nu Z_s$; the proportionality constant ν is called the resonator constant.[36] To measure f_0 and Γ, we use a source with narrow bandwidth (significantly smaller than Γ of the cavity) that operates at the central frequency of the cavity. The coupling of the source frequency F to f_0 is achieved by modulating the source frequency around F; a detection of the in-phase amplitude of the transmitted signal at the modulation frequency will measure the derivative of the cavity absorption spectrum, and be proportional to the error $\epsilon = (F - f_0)$ at first order. Then ϵ is fed back into the source. This arrangement is similar to the AFC (automatic frequency control) used, for example, in electron spin resonance methods. Here, we measure both f_0 with a frequency counter and the bandwidth Γ by measuring the value of the transmitted power at f_0; Γ is proportional to the inverse square root of the absorption curve maximum and thus $A(f_0) \propto \Gamma^{-2}$. To measure $A(f_0)$, we have the microwave power chopped and we use another phase-sensitive detection to analyze the signal transmitted. The chopping frequency is three orders of magnitude higher than the frequency of modulation to avoid mixing contributions induced by higher order nonlinearities. A schematic layout of the setup is shown in Fig. 2.

The measurement configuration used the so-called end plate technique, where one of the Cu end plates of the cavity is replaced by the sample. This scheme has the advantage over other possible experimental configurations in that no assumption is needed on the sample size or geometry (no depolarization factor is involved), which simplifies the analysis. Our experiments have been performed with a bulk sample of Nb and Pb cut in a flat disk of 10 mm diameter and 5 mm height, with a polished face that replaced the copper end plate and formed a wall of the cavity. For the TE_{011} mode, the resonator constant of the end plate is given by the expression $\nu = (c^3\pi^2)/(h^3\omega^3) = 0.0458$, where h is the height of the cavity.

The measurement protocol has been conducted as follows. The frequency of resonance f_0 and the half-width Γ are measured as a function of the temperature in two separate runs one before and one after the replacement of the copper (Cu) end plate by the sample (s). The difference is related to Z_s, the surface impedance of the sample, through the relation

$$\frac{f_s - f_{Cu}}{f_{Cu}} - i\frac{\Gamma_s - \Gamma_{Cu}}{2f_{Cu}} = -i\nu(Z_s - Z_{Cu}), \qquad (5)$$

where Z_{Cu} is the surface impedance of the Cu end plate only. We have calculated the ratio of the losses in the end
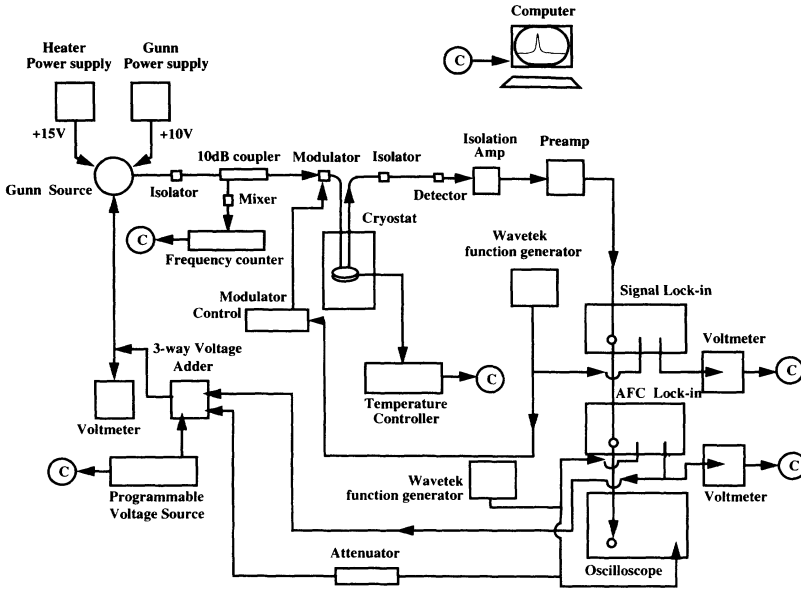
FIG. 2.   Experimental setup used to measure the surface impedance. Notice the feedback loop.

plate compared with the total losses at all the other surfaces of the empty resonator, assuming that only Ohmic effects are important. This ratio is independent of the conductivity of copper and is equal to 39% for our cylindrical cavity:

$$\frac{\Gamma_s - 0.61\Gamma_{Cu}}{2f_{Cu}} = \nu R_s. \tag{6}$$

Radiative losses through the coupling hole give an additional loss. In the analysis, after the subtraction of the Cu impedance, a small offset (less than 5%) is left as a free parameter to account for this additive term such that R_s of the superconductor is adjusted to be zero at the lowest temperature.

Also one cannot make an absolute measurement of Δf in the form defined by Eq. (5), as the end plate must be removed between the runs. Since the frequency is proportional to the volume of the cavity, it is extremely sensitive to the precise position of the walls. Due to mechanical uncertainties, it is not possible to place the end plate exactly in the same position after each removal, and the frequency shift $f_s - f_{Cu}$ can be measured only up to a numerical additive constant f_a. Because of the unknown f_a, some assumption had to be made for either the properties of the normal or superconducting state (see the discussion below).

IV. EXPERIMENTAL RESULTS

We discuss the results obtained in Nb and in Pb separately. As will be shown later, the electrodynamics of these two materials is somewhat different. The Nb used in this study was a bulk piece of 99.9% purity. In the preparation, the metal piece was etched with nitric acid, in order to remove the oxide layer at the surface and one surface was polished using a diamond polishing cream down to 0.3 μm. The Pb of 99.99% purity had its acid etched surface (used as the wall of the cavity) freshly polished down to 0.05 μm, using an alumina permanent

suspension abrasive cream. We took care that the surface of our sample is flat on the scale of $1/\mathrm{Im}(\hat{k})$.

A. Nb

In Fig. 3 the temperature dependence of both R_s and X_s is shown down to $T/T_c \sim 0.25$. The data are normalized to the normal state value (given below). For the analysis, we have assumed that the specimen was in the local limit, as supported by earlier measurements of Blaschke and Blocksdorf in 1982.[38] In this case the field decays exponentially as it penetrates in the sample and the surface impedance is the refractive index, $Z_s = \sqrt{\omega/4\pi i \hat{\sigma}}$. In the normal state, $\sigma_1 \gg \sigma_2$ in the mm-wave range, and $1/\mathrm{Im}(\hat{k})$ is called the classical skin
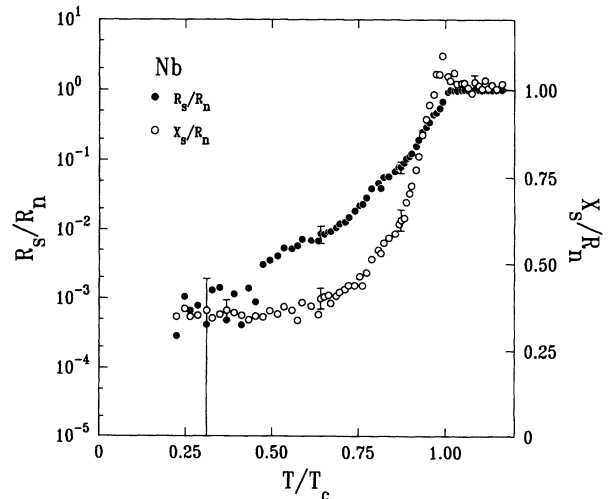
FIG. 3.   Temperature dependence of the surface resistance R_s and the surface reactance X_s of Nb. The surface resistance is displayed on a logarithmic scale while the surface reactance is plotted on a linear scale.

depth, defined as

$$\delta = \frac{c}{\sqrt{2\pi\omega\sigma_1}}.$$ (7)

Above T_c the surface resistance has the simple form

$$R_s = X_s = \frac{\omega}{c}\frac{\delta}{2},$$ (8)

and we use the latter equality to evaluate the unknown frequency offset f_a. In the normal state we find that R_s and X_s have the same temperature dependence, confirming the validity of the assumption, Eq. (8), in the entire measured temperature range.

Using the measured value of the half-width, we have calculated the normal state surface resistance $R_n = 0.0538 \ \Omega$ at $T = 10$ K. This result leads to a conductivity σ_n (10 K) $= 0.85 \times 10^6 \Omega^{-1} \mathrm{cm}^{-1}$, a value 3 times lower than the conductivity measured on single crystals ($\sigma_n = 2.9 \times 10^6 \Omega^{-1} \mathrm{cm}^{-1}$),[39] implying that our sample is well into the local limit. Using this conductivity, the skin depth at 10 K is $\delta = 2270$ Å. The surface resistance $R_s(T)$ drops rapidly with decreasing temperature and it is plotted on a logarithmic scale in Fig. 3. The scatter of data, 0.05 mΩ, is independent of the temperature and the value gives the resolution of our measurement configuration. We have subtracted a positive constant of 2 mΩ from the R_s data; this offset is attributed to the coupling losses not taken into account by Eq. (6). Careful measurements of the residual surface resistance were obtained with a different setup. Instead of using the end plate technique we have placed a small Nb superconducting sample at the bottom of the same Cu cavity (antinode of the magnetic field). In this configuration, Eq. (5) is modified and the right-hand side is simply equal to $-i\nu Z_s$. It was found that the residual R_s at $T/T_c \sim 0.25$ was 0.2 mΩ. There is a further uncertainty in the measurement of the absolute value of the loss: It originates from the dismantling of the cavity end plate after each run. This gives a reproducibility of ~ 0.1 mΩ.

Far below T_c, the temperature dependence of the surface reactance, X_s, is directly proportional to the temperature dependence of the penetration depth $\lambda(T)$. Using Eq. (8), we can deduce from Fig. 3 the zero temperature value of the penetration depth

$$\frac{X_s(0)}{R_n} = \frac{2\lambda(0)}{\delta}.$$ (9)

This result gives a penetration depth $\lambda(0) = 440$ Å, a result in good agreement with the value measured by Maxfield and McLean[40] (470 Å). Using the Fermi velocity $v_F = 0.15 \times 10^8$ cm sec^{-1} (Ref. 38) and the plasma frequency $\omega_P = \lambda_L/c$ (see London penetration depth value below), we estimate from σ_1 the mean free path $\ell \sim 200$ Å at $T = 10$ K. From the London penetration depth value $\lambda_L = 330$ Å (Ref. 38) and the BCS coherence length, $\xi_0 = 380$ Å, where the BCS gap $\Delta(0) = 1.4$ meV (see below) in Eq. (1), one can calculate the penetration depth in the local limit, including mean free path corrections. This gives $\lambda = \lambda_L\sqrt{\xi_0/\ell} = 450$ Å in good agreement with our earlier evaluation.

B. Pb

Pb is a type I superconductor with $\xi(0) > \lambda(0)$. Critical magnetic field measurements[41] have given a ratio $\xi(0)/\lambda(0) \sim 2$, suggesting that the material is not strongly in the Pippard limit; nevertheless we have used this limit to analyze the data; this approximation was also suggested by Nam.[9] The analysis in the local limit was published previously.[42] In the normal state of the anomalous limit,

$$R_s = \frac{X_s}{\sqrt{3}} = \frac{2\pi\omega}{c^2}\left(\frac{c^2\ell}{2\pi\alpha\sigma_1\omega}\right)^{1/3},$$ (10)

and the skin depth expression becomes

$$\delta^3 = \frac{c^2\ell}{2\pi\alpha\sigma_1\omega}.$$ (11)

The factor α was computed by Reuter and Sondheimer in 1948 (Ref. 43) for both specular scattering ($\alpha = 3^{11/2}\pi/128 \sim 10$) and diffuse scattering ($\alpha = 4\pi/\sqrt{3} \sim 7$). A simplified picture is to suppose that only a fraction $\alpha\delta/\ell$ of the electrons are effective in the conductivity.

We display in Fig. 4 the surface impedance in the superconducting phase. The onset of the surface resistance drop is at 7.2 K, the transition temperature. This value is in agreement with the onset temperature of the shielding diamagnetism in our measurement of the ac susceptibility. First, we note that the normalized value of both the surface resistance and the surface reactance of Pb are larger than what was obtained in the case of Nb, although the single particle gap and the frequency are comparable. At $T = 8$ K, $R_n = 0.0421 \ \Omega$ and this value gives a conductivity $\sigma_n = 1.4 \times 10^6 \Omega^{-1} \mathrm{cm}^{-1}$ and thus a skin depth, $\delta = 1780$ Å, using Eq. (11). The same consideration about errors that we made on the
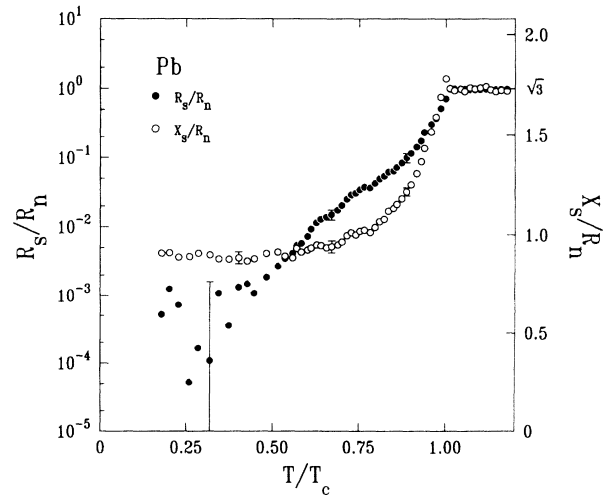
FIG. 4. Temperature dependence of the surface resistance R_s and the surface reactance X_s of Pb. The surface resistance is displayed on a logarithmic scale while the surface reactance is plotted on a linear scale.

TABLE I. Electrodynamic properties of Nb and Pb measured at 60 GHz; the v_F values are after Refs. 38, 3.

	T_c [K]	R_n [Ω]	σ_n [Ω^{-1} cm^{-1}]	δ [Å]	λ [Å]	v_F [cm sec^{-1}]	ℓ [Å]	$\xi(0)$ [Å]	Δ [meV]
Nb	9.3	0.0538	0.85×10^6	2270	440	0.15×10^8	200	380	1.4
Pb	7.2	0.0421	1.40×10^6	1780	380	0.42×10^8	2000	830	1.3

Nb behavior of $R_s(T)$ applies here. Our measured conductivity is much higher than the value obtained by Lehoczky and Briscoe ($\sigma_n \sim 3 \times 10^4 \Omega^{-1}$ cm^{-1}),[18] but comparable to the value listed by Blaschke and Blocksdorf ($\sigma_n = 1.1 \times 10^6 \Omega^{-1}$ cm^{-1}).[38]

Using the optical value of the plasma frequency[3] we estimate $\ell = 4\pi\sigma_n v_F / \omega_p^2 \sim 2000$ Å just above T_c. We have used a Fermi velocity $v_F = 0.50 \times 10^8$ cm sec^{-1} after Ref. 41 (p. 243) or Ref. 38. This indicates that the sample is at the border of the clean limit, with $\ell/\pi\xi(0) \sim 1$.

In the limit $T \ll T_c$, the surface reactance $X_s(T)$ is proportional to the penetration depth $\lambda(T)$ in the Pippard limit, but in the normal state X_s is not simply related to the skin depth. It can be shown that in the anomalous limit

$$\frac{X_s(0)}{R_n} \sim \frac{4.5\lambda(0)}{\delta}. \tag{12}$$

From the saturation value of the surface reactance at low temperature we estimate $\lambda(0) = 380$ Å, comparable to the value observed by Faber and Pippard ($\lambda = 390$ Å).[44]

To conclude this section, we have listed the measured (60 GHz) electrodynamic properties of Nb and Pb in Table I.

V. ANALYSIS

A. Nb

Using the measured value of R_s and X_s, we have evaluated the temperature dependence of the complex conductivity in the local limit. We display the results in Fig. 5. The real part of the conductivity σ_1 shows a peak that we attribute to the case 2 coherence factors. The position of the maximum is well below T_c where R_s is already several orders of magnitude lower than its normal state value at the peak maximum, and therefore the increase of σ_1 is clearly not due to the normal state or fluctuation effects.

The solid curves are the Mattis-Bardeen weak-coupling [$\Delta(0)/k_B T_c = 1.76$] calculation of the complex conductivity for a superconductor where no fitting parameter has been used. Note that the agreement between the solid curve and the experimental data points is good on the entire temperature range, indicating that Nb falls in the weak-coupling limit. The error bars in Fig. 5 do not reflect the scatter of data points but rather the systematic error caused by the change of the residual R_s value, ~ 2 mΩ (estimated in the previous section).

We have displayed on the same figure the temperature dependence of the imaginary part of the conductivity. From this measurement one can evaluate the temperature dependence of the superconducting gap. Using Nam's results in the local limit we find that[8]

$$\frac{\lambda_L}{\lambda} = \sqrt{\frac{\ell}{\xi(0)}} S, \tag{13}$$

where S is given by the following expression:

$$S = \frac{\Delta(T)}{\Delta(0)} \tanh \frac{\Delta(T)}{2k_B T} \tag{14}$$

or

$$\frac{\sigma_2}{\sigma_n} = \frac{\pi\Delta(T)}{\hbar\omega} \tanh \frac{\Delta(T)}{2k_B T}. \tag{15}$$

By inverting the last expression one can deduce the temperature dependence of the BCS gap. We display the result in Fig. 6, and compare it with the BCS self-consistent gap equation (solid line). Again, the agreement between the measurement and the theoretical prediction is ex-
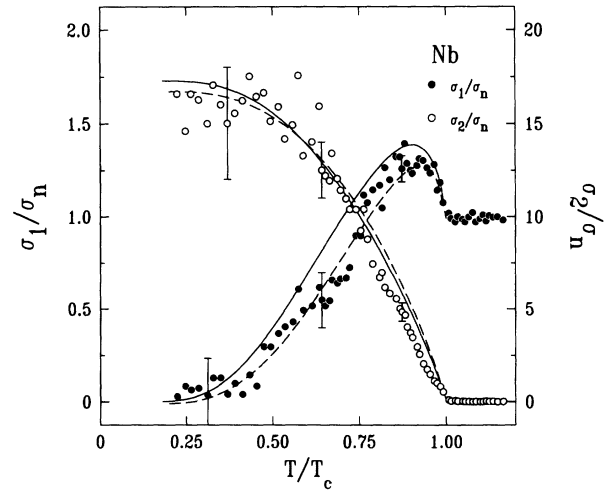
FIG. 5. Temperature dependence of the complex conductivity $\hat{\sigma} = \sigma_1 + i\sigma_2$ of Nb as evaluated from the surface impedance measurement. The solid curves are the weak-coupling Mattis-Bardeen prediction (Ref. 6). The dashed curves are the strong-coupling Eliashberg prediction, as discussed in the text.
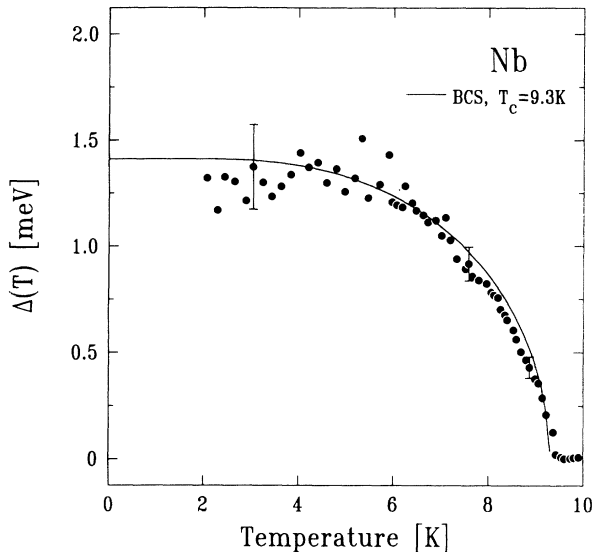
FIG. 6. Temperature dependence of the superconducting gap of Nb as evaluated using Eq. (15). The solid line is the gap, $\Delta(T)$, obtained in the weak-coupling BCS limit with $T_c = 9.3$ K.

FIG. 7. Temperature dependence of the complex conductivity $\hat{\sigma} = \sigma_1 + i\sigma_2$ of Pb as evaluated from the surface impedance measurement. The solid curves are the weak-coupling Mattis-Bardeen prediction (Ref. 6). The dashed curves are the strong-coupling Eliashberg prediction, as discussed in the text.

cellent. From our data, we infer a value for the single particle gap of Nb $\Delta(0) = 1.4 \pm 0.1$ meV.

Using Eq. (3), we also present in Fig. 5 the calculation for the complex conductivity calculated within Eliashberg theory (dashed curves). The $\alpha^2 F(\omega)$ is derived from tunneling measurements on Nb,[45] and the Coulomb pseudopotential is $\mu^* = 0.182$.[11] One finds the result is not very different from the weak-coupling BCS Mattis-Bardeen result, as expected for Nb. There does appear to be a slightly better fit to the data, which is expected as the Eliashberg calculation is an exact calculation which incorporates the modest strong-coupling effects in Nb. Again there are no free parameters in this calculation.

B. Pb

In Fig. 7 is shown the temperature dependence of the complex conductivity calculated from the surface impedance measurement using the Pippard limit. A peak is observed in the temperature dependence of σ_1, the maximum being well into the superconducting phase ruling out fluctuation effects [fluctuations are expected to be larger in Pb (Ref. 5) than in Nb]. The temperature (T_{max}) at the maximum of σ_1 is well below T_c and R_s (T_{max}) is an order of magnitude lower than R_n. Microwave transmission and reflection studies on thin films of superconducting Pb performed by Lehoczky and Briscoe[18] lead to the estimation that, at 60 GHz, the real part of the conductivity σ_1 at T_c exceeds by 4% the normal state value and the effect is attributed to fluctuations. In our experiment, fluctuations are within our measurement error and are much smaller than the height of our peak. The solid curve is the Mattis-Bardeen conductivity computed for Pb with $T_c = 7.2$ K. We observe

a large discrepancy between the theoretical and the measured temperature dependence. The width of the measured conductivity peak is significantly smaller than the predicted weak-coupling BCS value, indicating that Pb has a stronger coupling constant than the BCS one (cf. discussion in Sec. II).

However, calculating the conductivity with Eq. (3) using the tunneling $\alpha^2 F(\omega)$ and $\mu^* = 0.139$ of Pb (Refs. 46, 11) in a strong-coupling Eliashberg calculation greatly improves the agreement between theory and experiment, providing excellent confirmation of the strong-coupling effects in Pb. Once again this calculation has no free parameters. In particular, we note that due to the rapid opening of the gap (which is $2.25k_BT_c$ at $T = 0$ K compared to the BCS value of $1.76k_BT_c$), σ_1 decays faster with reducing temperature than the BCS weak-coupling limit. Likewise, σ_2 demonstrates a lower zero temperature limit: Strong coupling increases the zero temperature value of the penetration depth ($\sigma_2 \propto \lambda^{-3}$). The Eliashberg penetration depth exceeds by 8% the weak-coupling limit assuming the same value of the gap in both limits.

Nam extended the Mattis-Bardeen work for impure superconductors near the strong-coupling limit.[9] The penetration depth in the Pippard limit is given by the expression

$$\frac{\lambda_L}{\lambda} = \left[\frac{3\pi^2}{4}\frac{\lambda_L}{\xi(0)}S\right]^{1/3}, \tag{16}$$

where S is given by Eq. (14).

Using the previous equation, we have evaluated $\Delta(T)$ for Pb and plotted the result in Fig. 8. For comparison, we display on the same figure the BCS gap equation obtained for $T_c = 7.2$ K. At low temperature the measured
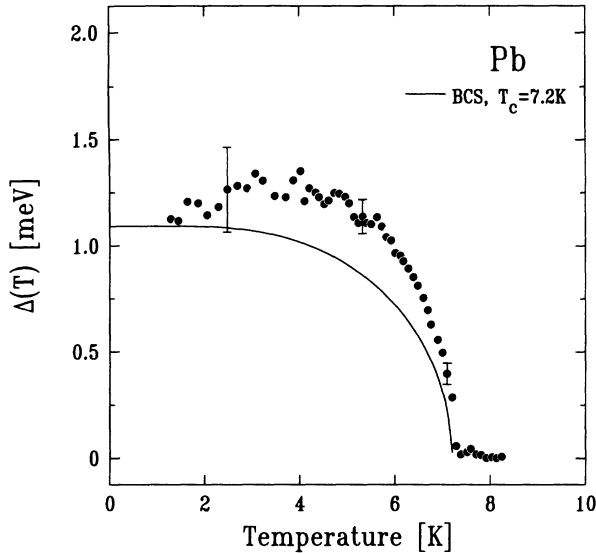
FIG. 8. Temperature dependence of the superconducting gap of Pb as evaluated using Eq. (16). The solid line is the gap, $\Delta(T)$, obtained in the weak-coupling BCS limit with T_c = 7.2 K.

gap of Pb exceeds by several tenths of meV the weak-coupling limit. From the data, we extrapolate the zero temperature value of the gap, $\Delta(0)$=1.3 meV, leading to a coupling constant $\Delta(0)/k_B T_c$ = 2.1. The result is also listed in Table I.

Finally, the temperature dependence of the penetra-
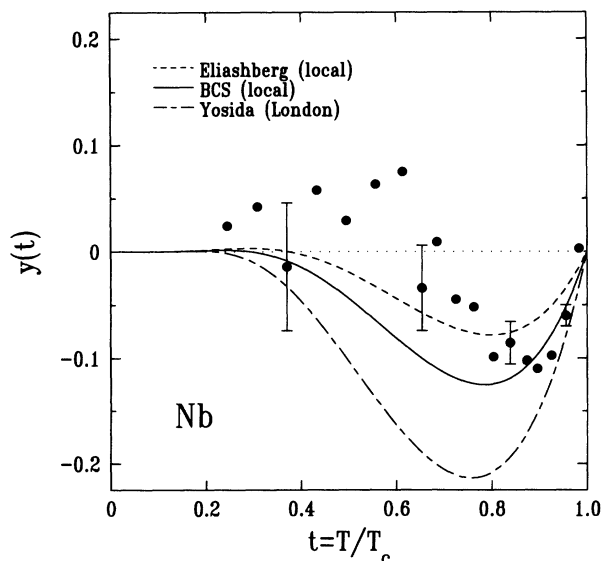
FIG. 9. Temperature dependence of the penetration depth for Nb. We have plotted the deviation from the two-fluid form, $y(T/T_c) = [\lambda(0)/\lambda(T)]^2 - [1 - (T/T_c)^4]$. The dot-dashed curve is the BCS Yosida function, the dashed curve is the result obtained for strong-coupling superconductors, and the solid curve is the BCS weak-coupling result in the local limit.
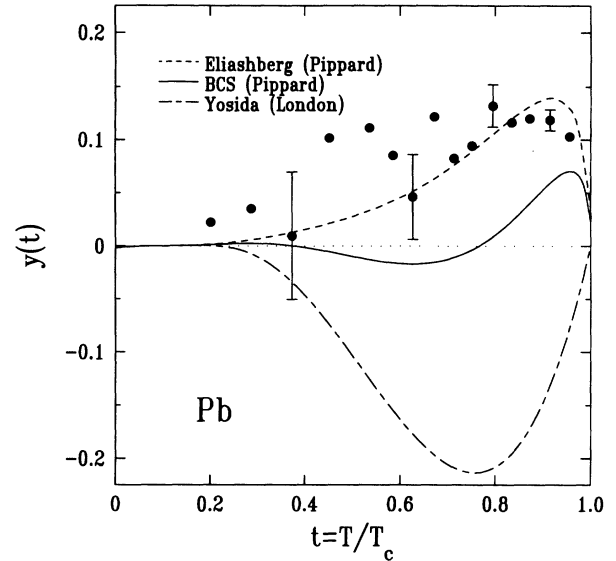
FIG. 10. Temperature dependence of the penetration depth for Pb. We have plotted the deviation of $[\lambda(0)/\lambda(T)]^2$ from the two-fluid form, $1 - (T/T_c)^4$. The dot-dashed curve is the BCS Yosida function, the dashed curve is the result obtained for strong-coupling superconductors, and the solid curve is the BCS weak-coupling result in the Pippard limit.

tion depth of Nb ($\lambda \propto 1/\text{Im}[(i\hat{\sigma})^{1/2}]$) and Pb ($\lambda \propto 1/\text{Im}[(-\hat{\sigma})^{1/3}]$) is displayed in Figs. 9 and 10, respectively. The data are shown as a deviation from the phenomenological two-fluid[47] expression. This empirical formula is used to approximate the electrodynamic response of strong-coupling superconductors.[24] We observe that neither of the results on Nb nor Pb are in agreement with the BCS weak-coupling Yosida function,[48] $\sum_k \partial f_k/\partial E_k$, where E_k is the energy of a quasiparticle of momentum k and f_k is its corresponding Fermi probability. Indeed, it is necessary to introduce the full strong-coupling calculations and the correct local or Pippard limit to account for our findings. The zero frequency, temperature-dependent penetration depths for Nb and Pb were calculated from an imaginary-frequency-axis formulation of the local and Pippard penetration depths, respectively, as given in Ref. 11. We also include the corresponding weak-coupling BCS curve for the local and Pippard limit. Clearly the data, particularly for Pb, are in better agreement with the strong-coupling result.

VI. CONCLUSION

We have reported results on the evaluation of the complex conductivity of Pb and Nb in the microwave range (60 GHz or 2 cm^{-1}) down to $T/T_c \sim 0.25$. The conductivity is inferred from the measurement of the two components of the surface impedance. Our experiments provide evidence for the existence of a peak in the conductivity below T_c, a signature of case 2 coherence fac-

tors. While Nb is in the weak-coupling local limit, for Pb strong-coupling corrections and nonlocal effects are evident. In the case of Nb, the temperature-dependent gap $\Delta(T)$ is in agreement with the BCS prediction. We have also demonstrated the necessity of using Eliashberg theory to describe strong-coupling superconductors, such as Pb.

*Present address: Physics Department, Massachusetts Institute of Technology, 77 Massachusetts Ave., Cambridge, MA 02139.

†Present address: Dept. of Physics, University of Guelph, Guelph, ON, N1G 2W1 Canada.

[1] J. Bardeen, L.N. Cooper, and J.R. Schrieffer, Phys. Rev. 108, 1175 (1957).

[2] J.R. Schrieffer, Theory of Superconductivity (Addison-Wesley, New York, 1988).

[3] R.E. Glover III and M. Tinkham, Phys. Rev. 108, 243 (1957); D.M. Ginsberg, P.L. Richards, and M. Tinkham, Phys. Rev. Lett. 3, 337 (1959); D.M. Ginsberg and M. Tinkham, Phys. Rev. 118, 990 (1960); P.L. Richards and M. Tinkham, ibid. 119, 575 (1960).

[4] L.H. Palmer and M. Tinkham, Phys. Rev. 165, 588 (1968).

[5] H.D. Drew and A.J. Sievers, Phys. Rev. Lett. 19, 697 (1967).

[6] D.C. Mattis and J. Bardeen, Phys. Rev. 111, 412 (1958).

[7] T. Holstein, Phys. Rev. 96, 535 (1954).

[8] S.B. Nam, Phys. Rev. 156, 470 (1967).

[9] S.B. Nam, Phys. Rev. 156, 487 (1967).

[10] G.M. Eliashberg, Zh. Eksp. Teor. Fiz. 38, 966 (1960) [Sov. Phys. JETP 11, 696 (1960)].

[11] J.P. Carbotte, Rev. Mod. Phys. 62, 1027 (1990).

[12] R.R. Joyce and P.L. Richards, Phys. Rev. Lett. 20, 1007 (1970).

[13] B. Farnsworth and T. Timusk, Phys. Rev. B 10, 2799 (1974).

[14] W. Shaw and J.C. Swihart, Phys. Rev. Lett. 20, 1000 (1968).

[15] P.B. Allen, Phys. Rev. B 3, 305 (1971).

[16] M.S. Khaikin, Zh. Eksp. Teor. Fiz. 34, 1389 [Sov. Phys. JETP 6, 961 (1958)].

[17] J.R. Waldram, Adv. Phys. 13, 1 (1964).

[18] S.L. Lehoczky and C.V. Briscoe, Phys. Rev. B 4, 3938 (1971).

[19] N.M. Rhugheimer, A. Lehoczky, and C.V. Briscoe, Phys. Rev. 154, 414 (1967).

[20] J. Halbritter, Z. Phys. 266, 209 (1974).

[21] L.C. Hebel and C.P. Slichter, Phys. Rev. 113, 1504 (1959).

[22] L.D. Landau and E.M. Lifschitz, Electrodynamics of Continuous Media (Pergamon, Oxford, 1984).

[23] P.G. de Gennes, Superconductivity of Metals and Alloys (Addison-Wesley, New York, 1989).

[24] M. Tinkham, Introduction to Superconductivity (McGraw-Hill, New York, 1975).

[25] L.C. Hebel, Phys. Rev. 116, 79 (1959).

[26] J.R. Schrieffer, D.J. Scalapino, and J.W. Wilkins, Phys. Rev. Lett. 10, 336 (1963).

[27] D.J. Scalapino, in Superconductivity, edited by R.D. Parks (Dekker, New York, 1969), p. 449.

[28] J.M. Daams and J.P. Carbotte, J. Low Temp. Phys. 43, 263 (1981).

[29] D. Rainer and G. Bergmann, J. Low Temp. Phys. 14, 501 (1974).

[30] F. Marsiglio, M. Schossman, and J.P. Carbotte, Phys. Rev. B 37, 4965 (1988).

[31] W. Lee, D. Rainer, and W. Zimmermann, Physica C 159, 535 (1989).

[32] N.E. Bickers, D.J. Scalapino, R.T. Collins, and Z. Schlesinger, Phys. Rev. B 42, 67 (1990).

[33] R. Akis and J.P. Carbotte, Solid State Commun. 79, 577 (1991).

[34] F. Marsiglio, Phys. Rev. B 44, 5373 (1991).

[35] A.M. Portis, D.W. Cooke, and E.R. Gray, J. Supercond. 3, 297 (1990).

[36] O. Klein, S. Donovan, M. Dressel, and G. Grüner, Int. J. Infrared Millimeter Waves 14, 2423 (1993).

[37] J.D. Jackson, Classical Electrodynamics (John Wiley & Sons, New York, 1975).

[38] R. Blaschke and R. Blocksdorf, Z. Phys. B 49, 99 (1982).

[39] R.G. Chambers, Proc. R. Soc. London A 215, 481 (1952).

[40] B.W. Maxfield and W.L. McLean, Phys. Rev. 139, A1515 (1965).

[41] J. Bardeen and J.R. Schrieffer, in Progress in Low Temperature Physics, edited by C.J. Gorter (North-Holland, Amsterdam, 1961), Vol. 3, p. 170.

[42] K. Holczer, O. Klein, and G. Grüner, Solid State Commun. 78, 875 (1991).

[43] G.E.H. Reuter and E.H. Sondheimer, Proc. R. Soc. London A 195, 336 (1948).

[44] T.E. Faber and A.B. Pippard, Proc. R. Soc. London A 231, 336 (1955).

[45] G.B. Arnold, J. Zasadzinski, J.W. Osmun, and E.L. Wolf, J. Low Temp. Phys. 40, 225 (1980).

[46] W.L. McMillan and J.M. Rowell, Phys. Rev. Lett. 14, 108 (1965).

[47] C.J. Gorter and H.B.G. Casimir, Z. Phys. 35, 963 (1934).

[48] K. Yosida, Phys. Rev. 110, 769 (1958).